University of Sistan and Baluchestan

Chemical Process Design

Available online at http://cpd.usb.ac.ir/

Mathematical Modeling of Multi-Effect Desalination System with Direct Solar Radiation

Sayyed Aboozar Fanaee[1]✉, Meysam Mahmoudi[2], Sajjad Nejad-Naghi[3]

[1] Corresponding Author, Department of Mechanical Engineering, University of Birjand, Birjand, Iran. Email: sab.famech@birjand.ac.ir
[2] Department of Mechanical Engineering, University of Birjand, Birjand, Iran. Email: meysam.mahmoudi@birjand.ac.ir
[3] Department of Mechanical Engineering, University of Birjand, Birjand, Iran. Email: Sajjad.nejadnaghi @birjand.ac.ir

ARTICLE INFO

Article type:
Research Article

Article history:
Received: 2026-02-09
Received in revised form: 2026-08-05
Accepted: 2026-08-17
Available online: 2026-08-17

Keywords: *Multi-Effect Distillation; Performance Ratio; Mathematical Model; Direct Solar Radiation*

ABSTRACT

Multi-effect distillation (MED) is one of the most widely used technologies for freshwater production in regions facing shortages of potable, agricultural, or industrial water, owing to its operation based on successive evaporation–condensation processes. This study investigates the effects of direct solar radiation and feed water temperature on the performance ratio of an MED desalination system. The novelty of this work lies in the direct and explicit coupling of solar radiation with the internal energy balances of the MED effects, allowing for a more realistic and fully coupled simulation of solar-assisted desalination performance. To this end, a precise numerical–algebraic hybrid approach capable of providing a fully parametric solution is employed. The mathematical model is developed based on the governing momentum, mass, and energy balance equations. The model predictions show good agreement with published data [8], with a maximum deviation of 0.1% observed at N=4 The results indicate that the performance ratio increases with the number of desalination effects under all investigated conditions. Under no-solar conditions, the highest performance ratio is obtained for a 12-effect system at 80 °C, reaching a value of 12.05, whereas the inclusion of solar radiation increases the performance ratio up to 14.56. Moreover, increasing solar radiation from 0 to 1100 W/m² enhances the performance ratio, with maximum increases of 22.1%, 20.1%, and 19.5% for systems with 4, 6, and 8 effects, respectively. A sensitivity assessment further confirms that the performance ratio is more responsive to variations in solar radiation than to changes in feed water temperature.

Cite this article: Fanaee, S. A., Mahmoudi, M., Nejad-Naghi, S., (2026), Mathematical Modeling of Multi-Effect Desalination System with Direct Solar Radiation Flux, *Chemical Process Design*, 4(2), 00-00. http//doi.org/10.22111/cpd.2026.54734.1085

DOI: http//doi.org/10.22111/cpd.2026.54734.1085

Publisher: University of Sistan and Baluchestan.

1. Introduction

Today, access to potable water has become a vital issue in many regions of the world, particularly in hot and arid areas such as the Middle East. Given that desalination processes are energy-intensive and costly, and considering the potential of various regions to harness suitable solar radiation, the necessity of utilizing sustainable resources is critically important. Recognizing the significance of energy consumption in desalination processes, selecting a method that consumes less energy or utilizes waste energy represents a suitable option from both economic and environmental perspectives [1]. As the demand for fresh water continues to rise, the need for developing and implementing desalination technologies across extensive areas is also increasing [2]. Furthermore, the growing demand for fresh water due to population growth, industrial development, and climate change has made the necessity for efficient desalination technologies more apparent than ever [3].

According to global experiences, the most widely used and principal methods of seawater desalination in medium to large volumes include reverse osmosis (RO), multi-effect distillation (MED), and flash evaporation, although reverse osmosis has a larger share globally [4]. Despite the advancements made in recent years in thermal methods, including reverse osmosis, there remains a need for thermal methods of desalination, particularly when seawater with high salinity, temperature, or pollution enters the desalination process. In this context, multi-effect distillation (MED) systems have garnered significant attention as a sustainable and scalable technology [5]. These systems are capable of producing high-quality fresh water from saline water sources by utilizing principles of heat transfer and staged evaporation [6]. The primary advantage of the MED technology, compared to other methods such as reverse osmosis (RO), lies in its ability to operate with highly saline waters and significantly reduce issues related to fouling and membrane pollution [7].

In the thermal desalination process of multi-effect distillation (MED), the driving steam produced by an external source is injected into the evaporator tubes of the first stage. The feed water is sprayed onto the tubes of the first evaporator, where steam flows, causing part of it to evaporate. The steam generated in the first stage (secondary steam) moves to the second stage, and this process is repeated until the final stage. From the second stage onward, the secondary steam transfers part of its thermal energy to the feed water, converting it into fresh water. The only condition for this process is that the temperature of the steam produced in each stage must not fall below that of the feed water to ensure heat exchange between the feed water and the steam. MED processes are designed in three configurations: forward, backward, and parallel [8]. In backward-fed MED, the feed water enters the system from the last stage, which has the lowest temperature and pressure. The feed water and secondary steam move in opposite directions. A disadvantage of this method is that the highest amount of brine is located at the highest temperature, which hinders its use in seawater desalination. In forward-fed MED, the feed water enters from the first stage and flows in the same direction as the steam flow until the last stage. The main feature of this method is its ability to utilize high-temperature brine. However, this method has not been commercially employed in seawater desalination. In parallel-fed MED, the feed water enters the evaporators as separate streams perpendicular to them. In multi-effect distillers with forward feed, both the feed water and steam flow in the same direction. The incoming water goes to the first effect, which has the highest temperature, and then sequentially passes through all effects until reaching the last effect, after which it enters the final condenser. In multi-effect distillers with backward feed, the feed water and steam flow in opposite directions. The feed water flows from the final condenser to the last effect, which has the lowest temperature, and then passes through each effect until reaching the first one. The problem with this model is that the highest concentration of brine occurs in the first effect, which has the highest temperature, thereby increasing the risk of scaling. Another drawback of this model is the need for higher pressure to pump seawater from one effect to another, which raises operational and maintenance costs. There is also an increased risk of air leakage from pump connections in this model. The advantage of this model is that it does not require preheaters, thus resulting in lower capital costs compared to other models.

In parallel-flow multi-effect distillers, the feed water exiting from the final condenser is uniformly distributed across each stage. The most significant advantage of this model is its simplicity and lower scaling formation compared to forward-fed and backward-fed multi-effect distillation configurations. Numerous models of multi-effect distillers have been studied regarding how design and operational variables affect the parameters related to the costs of producing fresh water in the scientific literature [9].

Al-Sayed and Silver developed one of the first models for forward-fed multi-effect distillers, calculating the performance ratio and heat transfer surfaces using simplified thermodynamic assumptions [10]. Dasuki and El-Eitouni developed precise mathematical models to investigate how design and operational variables affect cost parameters related to the production of distillates from multi-effect distillers [8]. Darvish and colleagues examined various configurations of multi-effect distillers and determined the relationship between the performance ratio and the required heat transfer surface area [11]. A study by Derota et al. focused on modeling different configurations of multi-effect distillers with various flow patterns for distillates and steam streams, which were simultaneously optimized to determine the best flow patterns based on the flow pattern in conventional multi-effect distillers with forward feed. The results showed that optimizing flow patterns improved the performance of the process, and they studied the surface area of multi-effect distillers, presenting 14 models in which the conversion coefficient and steam consumption of the distillers were compared. Other published works have optimized the processes of multi-effect distillers [12]. Jyoti and Khanam developed a model for a multi-effect distiller system for various operational configurations such as steam splitting, flash condensation, and steam underflow. They optimized the number of flash tanks present in the system based on economic analysis. The result of this analysis led to system modifications that improved the economic steam percentage and reduced steam consumption [13].

Piasentino and Cardona proposed a thermal-economic analysis of a single-effect distiller to optimize a multi-effect distiller, leading to a deeper understanding of exergy relationships and fluid flow. As observed, improving the efficiency of heat exchangers in evaporators has thermodynamic limitations [14]. Zanoo et al. developed a steady-state mathematical model for a backward-feed multi-effect distillation (MED) system aimed at desalinating highly saline wastewater from a typical treatment plant. Their study focused on optimizing key operational and design parameters, including the number of effects, performance ratio (PR), steam flow rate, the minimum temperature difference between successive effects, and the overall economic performance of the process [15]. Al-Alawi investigated the impact of high brine temperatures and the number of effects (stages) on the efficiency of multi-effect distillers, analyzing the system energy output with and without steam thermal compression. Their results indicated that increasing the number of effects from three to six nearly doubled the obtained output ratio (GOR) [16]. Ely and El-Figy developed a steady-state mathematical model to investigate the performance of forward-fed multi-effect distillers, finding that the performance ratio was more dependent on the high brine temperature than on the number of stages [17]. Amiri and colleagues have also developed a thermodynamic model for a multi-effect distiller (MED) with a production capacity of 2111 cubic meters per day, detailing the impact of the number of stages on the performance indicators of the distiller [18]. Casimiro and colleagues modeled an evaporative distiller with a solar concentrator using TRNSYS software. In a similar study, they analyzed multi-effect distillers and solar concentrators for a Sicilian power plant [19-20]. Azimibayil and colleagues focused on the modeling and dynamic simulation of a multi-effect distillation system, extracting and addressing the influencing parameters [21].

Additionally, Mahan and colleagues conducted modeling and simulation of an (MED-TVC) process using HYSYS software [22]. Kamali and colleagues wrote a computer code for optimizing a multi-effect distiller with a thermal vapor compressor to achieve maximum possible output rates and reduce power consumption, using it for a sample with a daily capacity of 1500 cubic meters of fresh water [23]. Kamali and Mohabeniya optimized a multi-effect distillation unit with a thermal vapor compressor on Qeshm Island based on the design of evaporators, thermo-compressors, injectors, and ultimately simulating the entire cycle of the distiller, presenting algorithms [24]. Abdi Khanqah and colleagues utilized mathematical modeling to design and optimize a (MED-TVC) distiller for installation in the Persian Gulf. Their results indicated that increasing the driving steam pressure led to a decrease in GOR, while increasing the feed water temperature and steam flow rate resulted in an increase in GOR [25]. Ahmadinejad and colleagues conducted a simulation and economic analysis of desalination using the (MED-TVC) method in a power plant located on Kish Island, aiming to reduce carbon dioxide levels in the atmosphere and simultaneously produce fresh water and electricity from the waste energy in the compressor (the largest amount of wasted energy in the power plant). Their results indicate that the proposed cycle has favorable economic conditions over one year [26].

Ghorbani and colleagues investigated the parametric analysis and multi-objective optimization of a three-stage desalination system with a steam ejector, finding that increasing the temperature of the input steam enhanced fresh water production and the energy efficiency of the system. They also concluded that the lowest and highest costs in a year were related to the ejector and the second stage of the distiller, respectively [27]. Sayadi and Safari developed a model of an (MED-TVC) distiller and optimized it using thermo-economic analysis; the developed model was related to one of the distillers on Kish Island, which was selected for their study [28-29]. Al-Abidi and colleagues focused on the dynamic modeling of (MED) systems under variable operational conditions (such as temperature and salinity variations of the input water). By employing optimization algorithms, the researchers achieved a 25% reduction in specific energy consumption. This study also demonstrated that adjusting operational parameters in real-time could enhance system performance under unfavorable conditions [30]. Palenzuela et al. developed a steady-state mathematical model for a vertically stacked, forward-feed multi-effect distillation (MED) system, validated against experimental data from the pilot plant at the Plataforma Solar de Almería (PSA). Their study demonstrated that the model is both computationally efficient and suitable for the optimization of water production in cogeneration systems, achieving a high degree of accuracy with a maximum prediction error of 9% [31].

Zaman and colleagues conducted thermodynamic modeling and exergy analysis of a (MED) system connected to a steam power plant. By recovering heat from waste streams (condensate), they determined the optimal temperature for the driving steam, significantly increasing the rate of production (GOR) and reducing the cost of produced water by 18% [32]. Shahouni et al. sought to optimize and solve the environmental challenges of MED-TVC desalination systems in areas with insufficient sunlight and unstable weather conditions. They presented a model for using electric heaters as an alternative thermal energy source alongside the MED-TVC system. The optimization of their proposed system included adding an additional ejector in the last stage to improve the discharge of non-distillable gases and increase water production. Their results showed that the design of specific heating elements increased the heat transfer coefficient and reduced the pressure drop, and their economic analysis also showed that the direct cost of using electric heaters is significantly lower than using parabolic trough solar collectors, and the proposed system has higher efficiency and is more economical [33].

In Khonsha, CFD was used to investigate pressure and velocity distributions in a spinning cone column under dry and two-phase conditions. The results showed that increasing gas flow rate increases pressure drop, while the improved geometric model enhanced agreement with experimental data. These findings highlight the potential of CFD for analyzing and optimizing heat and mass transfer in thermal desalination systems, particularly multi-effect distillation (MED) units [34]. In a recent study, Karishma and Jana developed a dynamic modeling and multi-objective optimization framework for a multi-effect desalination system with thermal vapor compression (MED–TVC) in a parallel cross-feed configuration. The model was validated using operational data from large-scale desalination plants and employed to analyze trade-offs among performance ratio, freshwater production cost, and environmental impact. The findings demonstrated that the choice of optimization algorithm significantly influences the balance between efficiency, cost, and sustainability in MED–TVC systems. [35].

Most previous studies have focused on freshwater production using waste heat from power plants and renewable energy sources to provide the thermal energy required for operating multi-effect desalination systems. However, the approach of increasing the feed water temperature for each effect using independent thermal sources has not been extensively examined. Hence, the present study focuses on desalinating brackish water by applying direct solar radiation to each effect of a multi-effect desalination unit, with developing a comprehensive mathematical model.

2. Physical model

The schematic of proposed multi-effect desalination (MED) system designed in this study is presented in Fig. 1. To enhance efficiency and increase the freshwater production rate, direct solar radiation is considered as an integral factor influencing system performance. The position of inlet and outlet streams for a single stage are depicted in Fig. 2.

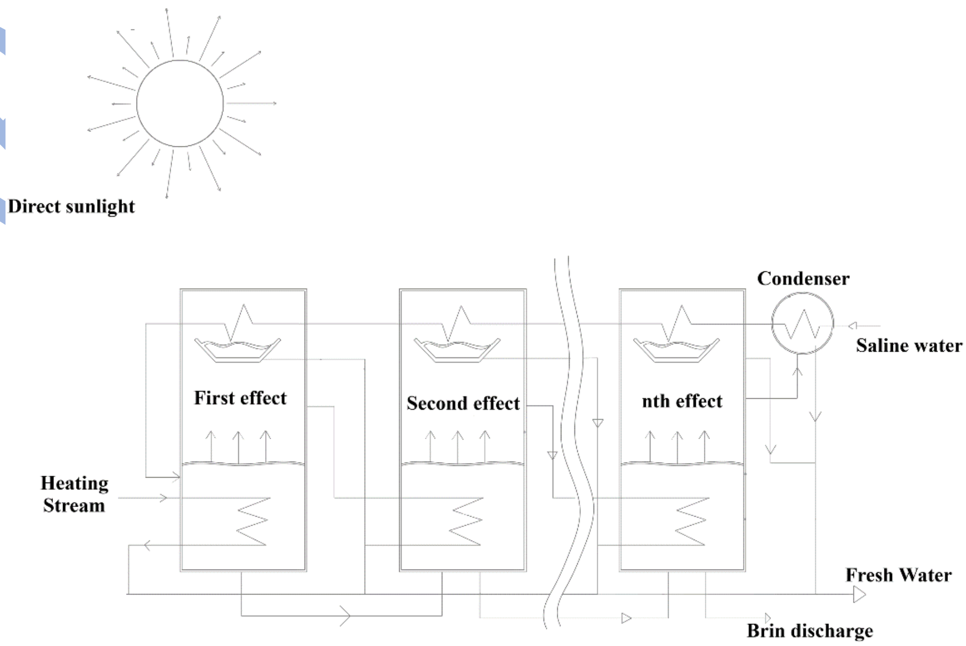

Fig. 1. Proposed MED system with direct solar radiation flux on effect chambers

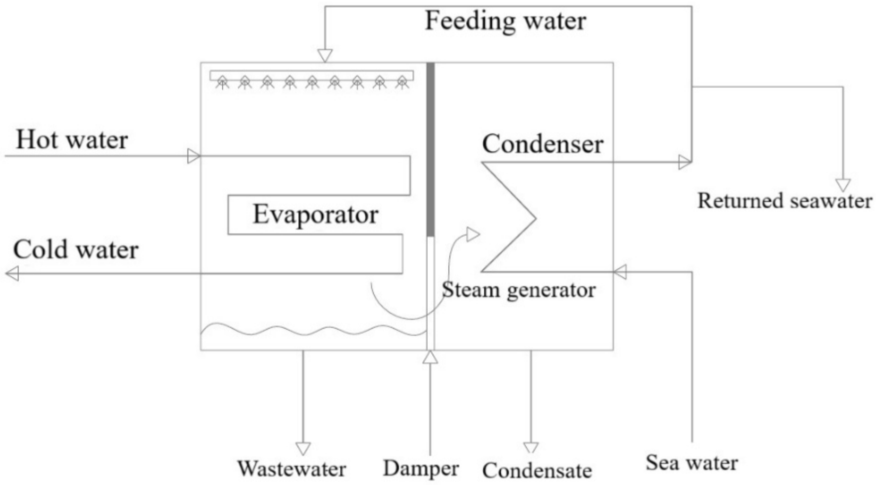

Fig. 2. Inlet and outlet streams for a single effect

The specifications of the multi-effect desalination (MED) system and the corresponding operating parameters are summarized in Table 1. The main input parameters considered in the present study include the number of effects (N), seawater salinity (X_f), steam temperature (T_S), the corresponding steam pressure (P_S), motive steam mass flow rate (M_d), and the overall temperature loss (ΔT_{loss}). As listed in Table 1, the steam temperature is fixed at 200 °C, while the motive steam mass flow rate varies in the range of 1–2 kg/s. The seawater salinity is assumed to be 42,000 ppm, and the total temperature loss across the system is taken as 2 °C. In addition, the number of effects is varied from 4 to 12 in order to investigate its influence on the system performance. These selected parameter values are used as the baseline conditions for the mathematical modeling and performance analysis of the MED system.

Table 1. Specifications of the Present MED System

Parameter	T_S	P_S	M_d	X_f	ΔT_{loss}	N
Value	200 °C	1554.9 kPa (abs)	1-2 kg/s	42000 ppm	2 °C	4-12

3. Mathematical model

The mathematical model is based on mass conservation, energy conservation, and heat transfer equations, along with correlations for heat transfer coefficients and the physical properties of water. To model the system, mass and energy balance equations are formulated for each stage, entire system, and the condenser. The equations are solved using known parameters and system constants, allowing the evaluation of different performance factors. Additionally, relations for calculating energy consumption and system efficiency criteria are derived. The fluid in the MED system is consisted of two components of pure water and salt. Therefore, the system's energy analysis is divided into thermomechanical and chemical parts.

The temperature difference between each two effects is calculated as follows:

$$T = \frac{T_1 - T_n}{N - 1} \quad (1)$$

The difference between temperatures of each effect with the previous one is equal to ΔT. Therefore, if the temperature at effect i is T_i, the temperature at effect i+1 is determined by the following equation:

$$T_i = T_{i+1} + T \quad (2)$$

The temperature of the vapor produced in effect *i*, denoted as T_{vi}, is lower than the saturation temperature for saline water with difference of the boiling point elevation (BPE). In this model, BPE in each effect is considered as a function of the temperature and salinity of the feed water, which presented as follows [8]:

$$BPE = A.X + BX^2 + C.X^3 \tag{3}$$

$$A = 80325\times10^{(-2)} + 1.883\times10^{(-4)}\times T + 4.02\times10^{(-6)}\times T^2$$

$$B = -7.62\times10^{(-4)} + 9.02\times10^{(-5)}\times T - 5.2\times10^{(-7)}\times T^2$$

$$T_{vi} = T_i - BPE \tag{4}$$

Since a demister is installed in each effect to prevent brine droplet entrainment, the generated vapor passes through the demister after the evaporation process. This passage causes a pressure drop across the demister, which in turn leads to a reduction in the vapor saturation temperature. The vapor then flows to the subsequent effect at a lower temperature

$$T_{evi} = T_{VI} - T_P \tag{5}$$

The flow rate of feed water from the sea for each effect is represented by F_i that is calculated as follows:

$$F_i = \frac{M_f}{N} \tag{6}$$

In all effects, the brine rejected from effect *i* enters effect *i*+1, and in last effect this water is discharged. The brine discharge rate from each effect is given by the following equations:

$$B_1 = F_1 - D_1$$

$$B_{(i+1)} = \sum_{(i=1)}^{(i+1)} F_i - D_i \qquad (i = 1, \text{n}.., N-1) \tag{7}$$

To formulate the energy balance equations, the latent heat of vaporization needs to be calculated. This is determined using empirical equations as a function of temperature.

$$\lambda = 2501.9 - 2.407\times T + 0.00119\times T^2 - 1.5863\times10^{-5}\times T^3 \tag{8}$$

By writing and rearranging the energy balance equations for the first effect, the vapor generated due to boiling can be obtained as:

$$D_1 = \frac{(M_m + M_{ev}).\lambda_s - F_1.C_p.(T_1 - T_f)}{\lambda_1} \tag{9}$$

where in this equation, *M* represents the mass flow rate of the driving steam, M_{iv} denotes the mass flow rate of the saturated vapor extracted from the last effect into the ejector, λ_S is the latent heat of vaporization at temperature T_I, λ_I is the latent heat of vaporization at the inlet temperature. For the second effect, the energy balance equation allows the calculation of the mass of vapor produced as:

$$D_2 = \frac{D_1.\lambda_1 - F_2.C_p.(T_2 - T_f) + B_1.C_p(T_1 - T_2)}{\lambda_2} \tag{10}$$

The equation extends similarly for all later effects as follows:

$$D_i = \frac{(D_{i-1}.\lambda_{i-1} + d_{i-1}.\lambda_{i-1} + d'_{i-1}.\lambda'_{i-1})}{\lambda_i} + \frac{F.C_p(T_i - T_f) + i.p.(i-f)}{\lambda_i} + \frac{B_{i-1}.C_p.(T_{i-1} - T_i)}{\lambda_i}\ ,\ i = 2,\ \dots, N \tag{11}$$

In the above relations, d_1 and d'_1 denote the mass flow rates of saturated vapor generated by flash evaporation in the brine reject and the corresponding condensed water in each stage, respectively. The variables D_i and D_{i-1} refer to the distillate flow rates in the *iii*-th and ($i-1$) th effects, respectively, whereas F, B_{i-1}, C_p , λ_i , T_f , T_i , T_{i-1}, T'_{i-1} and T''_i represent the feed and brine flow rates, heat capacity, latent heat terms, and temperature variables appearing in the MED mass and energy balances. The term $i.p$ appearing in Eq. (11) represents the absorbed solar radiation contribution at effect i, where I is the incident solar irradiance and α_p is the effective absorptivity of the effect surface (consistent with the I and α notation introduced earlier for the solar absorption terms); the product is multiplied by the local temperature difference ($T_i - T_f$) and normalized by the latent heat λ_i, exactly as defined for the solar terms in Eqs. (5)–(8) above. The parameters can be calculated as follows:

$$d_i = \frac{B_{i-1}.C_p.\left(T_{i-1} - T_i^{'}\right)}{\lambda_i^{'}}\ ,\quad i = 2,\ \ldots, N \tag{12}$$

$$d_i^{'} = D_i.C_p.\left(\frac{T_{i-1} - T_i^{''}}{\lambda_i^{'}}\right)\ ,\quad i = 2,\ \ldots, N \tag{13}$$

In Eq. (13), T'_1 represents the temperature of the liquid stream (brine or condensed distillate) entering the flash evaporation zone of the first effect. At this temperature, a portion of the liquid undergoes flash evaporation, and the corresponding latent heat of vaporization λ'_1 is used to calculate the amount of flash-generated vapor.

Since flash evaporation occurs under non-equilibrium thermodynamic conditions, the temperature of the generated vapor is slightly higher than the saturation temperature corresponding to the operating pressure of the effect. This deviation from equilibrium is accounted for by introducing the non-equilibrium allowance (NEA). Accordingly, for the first effect, the relationship between the liquid temperature and the vapor temperature is expressed as:

$$T_1^{'} = T_1 + NEA_1 \tag{14}$$

The non-equilibrium allowance in the first effect is evaluated using the following empirical correlation:

$$NEA_1 = \frac{0.33\left(T_0 - T_i\right)}{T_{v1}} \tag{15}$$

where T_0 denotes the temperature of the vapor entering the first effect from the upstream stage, and T_{v1} is the vapor temperature in the first effect. The temperature of the distilled water entering the flash evaporation process in the first effect is therefore obtained as:

$$T_1^{'} = T_{v1} + NEA_1 \tag{16}$$

The same formulation is applied sequentially to the second effect and all subsequent effects. For the second effect, the liquid temperature entering the flash evaporation zone is denoted by T'_2 and the non-equilibrium allowance is evaluated based on the temperature difference between the vapor leaving the first effect and the brine temperature of the second effect. In general, this approach ensures a consistent and physically realistic representation of the flash evaporation process throughout the entire multi-effect desalination system.

$$T_i^{'} = T_{vi} + NEA_i X_{b1} = \frac{F_1}{B_1}.X_f \tag{17}$$

Finally, the total amount of produced freshwater is determined by:

$$\mathrm{M_d} = \sum_{\mathrm{i=1}}^{\mathrm{n}} \mathrm{D_i} + \sum_{\mathrm{i=2}}^{\mathrm{n}} \mathrm{d_i} \tag{18}$$

To incorporate the effect of direct solar radiation, the absorbed energy is calculated as:

$$Q_{Solar} = I.A.\alpha.\tau \tag{19}$$

The temperature rise of the brine stream is then determined by:

$$T_{effect\,(new)} = T_{effect\,(old)} + \frac{Q_{Solar}}{\dot{m}C_p} \tag{20}$$

In the aforementioned equations, Q_{solar} represents the absorbed solar heat rate, while I, A, α, and τ denote the incident solar irradiance, effective surface area, surface absorptivity, and cover transmittance, respectively. Furthermore, $T_{effect(new)}$ and $T_{effect(old)}$ refer to the brine temperatures after and before the solar energy absorption, where $\dot{m}$ is the brine mass flow rate and C_p represents the specific heat capacity. It is important to note that Eq. (20) does not operate as a standalone correction appended to an otherwise independent solution. Once T_{inew} is established for each effect, it propagates through all subsequent temperature-dependent quantities: the boiling point elevation (Eq. (3)), the latent heat of vaporisation (Eq. (8)), and the enthalpy driving force ($T_{inew}-T_f$) in the distillate rate equations (Eqs. (9) and (11)). Consequently, the distillate flow rates D_1 through D_N, and the resulting performance ratio, reflect the fully updated thermal state of the system rather than a post-hoc adjustment to a pre-computed solution.

The performance ratio (PR), can be determined using following equation:

$$PR = \frac{M_d}{M_s} \tag{21}$$

where in this equation the parameter M_s is calculated as follows:

$$M_s = D_1 \frac{\lambda_{v1}}{\lambda_s} \tag{22}$$

The temperature difference between two consecutive stages is uniform and denoted as ΔT.

For solution of these equations, an algebraic code with considering a MATLAB module is adapted. The mathematical model that is included as facilitating and design of the MED desalination unit using direct solar radiation. Furthermore, to develop the solution some assumptions are established as follows:

1) The feed water enters each effect at an equal flow rate.
2) It is assumed that the vapor generated in each effect is salt-free, as the evaporation process involves only phase change of pure water, while dissolved salts remain in the liquid brine.
3) Temperature losses due to friction in connecting pipes and the condenser are neglected.
4) The system operates in steady-state conditions.
5) The surface area of each effect is equal.

4. Model validation

For validation of this model, a comparison between the calculated temperatures of each stage of MED desalination with numerical data [8] is presented for a six-effect MED system in Fig. 3. Given the accuracy of the computational code, the input parameters of the system are set according to Table 1. As seen in this figure, the results of the present algebraic model have an acceptable agreement with the published data [8] with maximum errors of 0.1% where this error is occurred in N=4. Furthermore, the trend of variation for temperature in the present model and numerical data [8] is unique. From the validation results in Fig. 3, it is observed that temperature decreases progressively across each effect. Since the temperature difference are very small, for a precise comparison, in Table 2, the extracted effect temperature from the algebraic calculations is presented in comparison to numerical one [8].

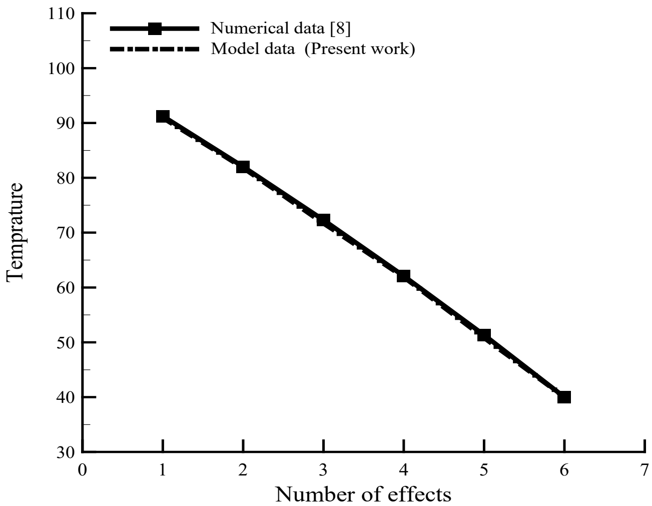

Fig. 3. Comparison of the effect temperature of the present study with numerical present data [8] under conditions of n = 6, T_S=100℃ ‹M_d =1 kg/s ‹X_f = 42000 ppm ‹X_6 = 70000 ppm

Table 2. The comparison of algebraic present effect temperature with numerical one [8]

Effect number	1	2	3	4	5	6
T (℃) The present study	91.2370	82.0133	72.3040	62.0829	51.3245	39.9989
T (℃) Reference [8]	91.2372	82.0132	72.3037	62.0831	51.3247	40

If solar radiation is adjusted so that the updated temperature in each effect does not experience a significant drop compared to the first effect – or even increases the temperature change within each effect – conditions can be created where the temperature rises throughout the effects. Consequently, the overall system efficiency will not only be maintained but it can also improve due to the influence of solar radiation.

Furthermore, an additional validation was performed by comparing the model results with the experimental data reported in reference [31]. Table 3 presents the brine mass flow rate leaving each effect, comparing the present study with the experimental values from [31]. The comparative analysis demonstrates excellent agreement between the model predictions and the experimental data, with a relative error of less than 1% for the investigated effects. This level of accuracy confirms the validity of the computational approach and demonstrates the model's reliability for precise thermodynamic analysis of the system.

Table 3. Comparison of brine mass flow rates between the current model and experimental data [31]

Effect No.	Present study (kg/s)	Experimental Reference [32] (kg/s)	Absolute error (kg/s)	Relative error (%)
1	2.151	2.149	0.002	0.093
2	2.082	2.079	0.003	0.144
3	2.014	2.011	0.003	0.149
4	1.948	1.944	0.004	0.206
5	1.883	1.878	0.005	0.266
6	1.821	1.813	0.008	0.441
Max	—	—	**0.008**	**0.441**
Mean	—	—	**0.004**	**0.217**

5. Results and discussion

One of the most important parameters for estimation of MED system is the performance ratio (PR), which is defined as the ratio of the produced freshwater to the amount of steam entering the first effect. In this study, each effect is assumed to be transparent so that the solar radiation increases the temperature. In this model, the inlet steam is compressed and enters the system at a temperature of 100 °C. Fig. 4 illustrates how the performance ratio varies with variation of the number of effects. As observed, the results show that the performance ratio increases with the number of effects under all examined conditions; however, the rate of increase depends on the feed water temperature and solar radiation level. The reason is that an increase in the number of effects leads to a reduction in the temperature difference between effects while increasing the overall effect temperatures. As a result, steam consumption decreases, ultimately improving the performance ratio. From the analysis of the effect, it is evident that a higher number of effects in an MED unit enhances the performance ratio. However, while adding more effects to the MED system poses a significant maintenance and operational cost challenge.

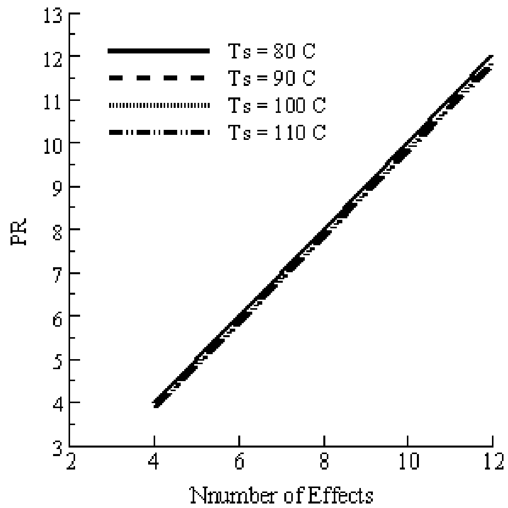

Fig. 4. Variation of the performance ratio as a function of the number of desalination effects for different feed water temperatures at a constant direct solar radiation intensity of 1000 W/m²

Fig. 5(a) and (b) illustrate the variations of PR versus the feed water temperature at different numbers of effects in the MED desalination system. These figures present the results for two cases: without and with 1000 W/m² direct solar radiation. As observed, increasing solar radiation enhances the performance ratio. The highest performance ratio is obtained in a 12-effect system at 80 ˚C, with a value of 12.05. Consequently, it is evident that intensifying solar radiation improves the performance ratio. The changes of feed water temperature are more pronounced in the presence of solar radiation than in its absence. This result is attributed to the fact that as the feed water temperature increases, the saturation potential of the incoming stream for vapor absorption decreases.

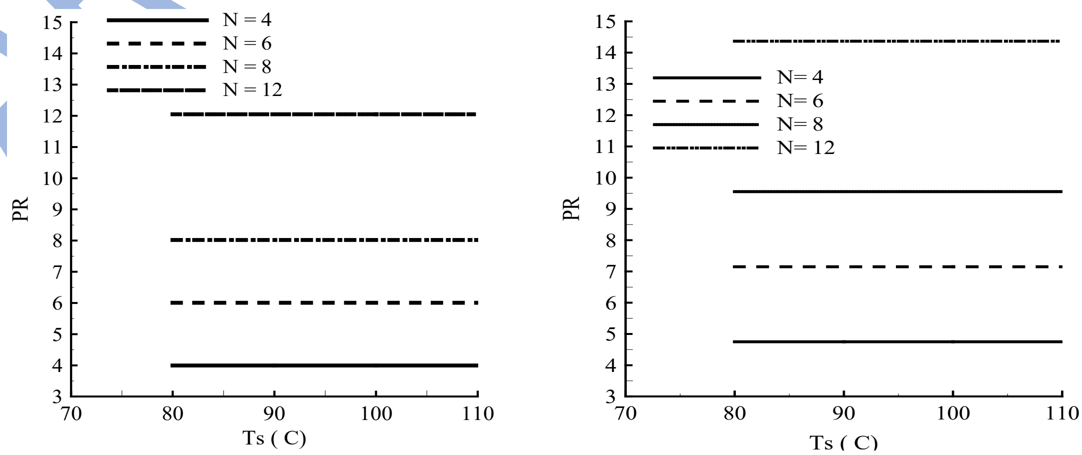

(a) (b)

Fig. 5. The variation of performance ratio versus feed water temperatures at different desalination effect with (a) $Q_{rad} = 0$ W/m² and (b) $Q_{rad} = 1000$ W/m²

Table 4 and Table 5 present the effect of variations in solar radiation on the pressure ratio value at different desalination effects at fixed feed water temperatures of T_s=80 °C and T_s=110 °C, respectively. As the solar radiation increases, the performance ratio improves across all configurations. The reason behind this improvement is that increasing solar radiation raises the temperature of each effect, which in turn enhances the overall performance ratio of the MED system. Furthermore, it is evident that increased solar radiation significantly enhances the system's efficiency. The maximum increase in PR is 20.3% for a feed water temperature of 80 °C and N=12.

Table 4. The variation of performance ratio (PR) versus solar radiation on the different desalination effect at a fixed feed water temperature of T_s=80 °C

Qrad (W/m²)	PR			
	N=4	N=6	N=8	N=12
0	4.00	6.01	8.02	12.05
800	4.62	6.96	9.29	13.97
900	4.69	7.06	9.42	14.17
1000	4.75	7.15	9.55	14.37
1100	4.81	7.25	9.68	14.56

Table 5. The variation of performance ratio (PR) versus solar radiation on the different desalination effect at a fixed feed water temperature of T_s=110 °C

Qrad (W/m²)	PR			
	N=4	N=6	N=8	N=12
0	3.91	5.89	7.88	11.85
800	4.55	6.87	9.19	13.84
900	4.62	6.97	9.32	14.05
1000	4.68	7.07	9.46	14.25
1100	4.75	7.17	9.59	14.45

Figs. (6), (7), and (8) present the variation of the performance ratio as a function of direct solar radiation for different feed water temperatures at fixed numbers of desalination effects equal to 4, 6, and 8, respectively. Fig. 6, corresponding to a four-effect desalination system, shows that increasing solar radiation leads to a noticeable improvement in the performance ratio for all feed water temperatures. The enhancement is more pronounced at lower feed water temperatures, indicating a stronger contribution of solar energy when the initial thermal potential of the feed stream is lower. Under these conditions, the maximum increase in the performance ratio reaches approximately 22.1%.

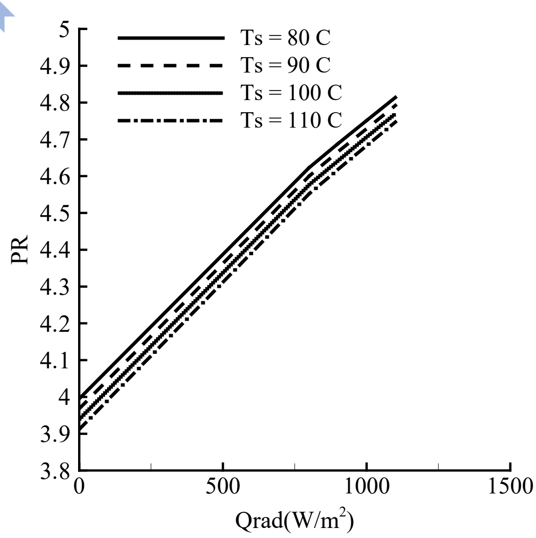

Fig. 6. The variation of performance ratio (PR) versus solar radiation on the different feed water temperatures for a fixed desalination effect of N=4

In Fig. 7, which represents a six-effect system, a similar increasing trend of the performance ratio with solar radiation is observed. However, compared to the four-effect configuration, the relative improvement becomes slightly lower, with a maximum increase of about 20.1%. This behavior can be attributed to the higher internal heat recovery within systems with a larger number of effects, which reduces the relative impact of additional solar input.

Fig. 8 illustrates the results for an eight-effect desalination system. Although the performance ratio still increases with solar radiation for all feed water temperatures, the marginal gain is further reduced compared to the previous cases. The maximum improvement in this configuration is approximately 19.5%, indicating that as the number of effects increases, the system becomes less sensitive to variations in solar radiation intensity.

Overall, the comparison of Figs. (6)–(8) demonstrates that while intensifying solar radiation consistently enhances the performance ratio, its relative impact diminishes with increasing number of desalination effects due to improved internal thermal efficiency of the multi-effect desalination system.

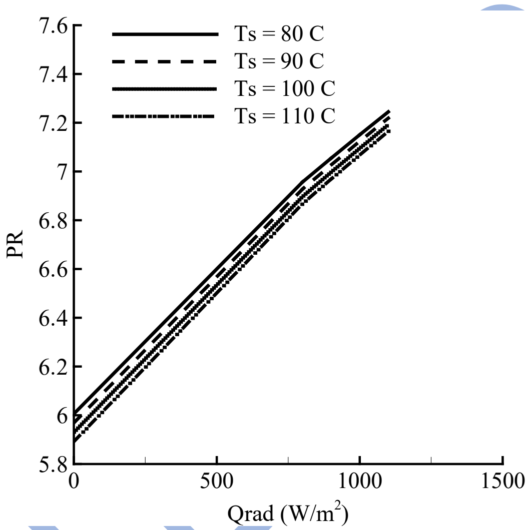

Fig. 7. The variation of performance ratio (PR) versus solar radiation on the different feed water temperatures for a fixed desalination effect of *N*=6

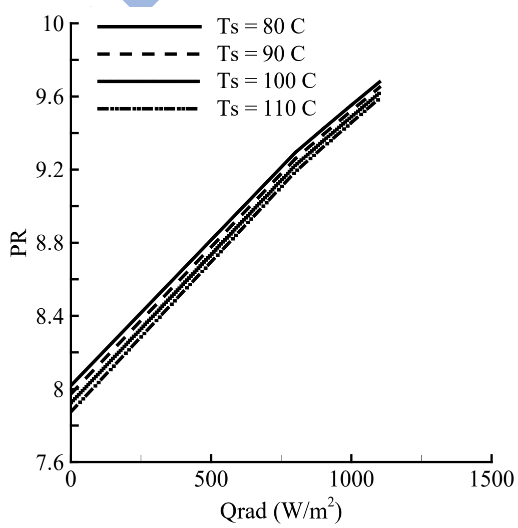

Fig. 8. The variation of performance ratio (PR) versus solar radiation on the different feed water temperatures for a fixed desalination effect of *N*=8

Tables (6), (7), and (8) illustrate the variation of the performance ratio as a function of direct solar radiation for different feed water temperatures, while maintaining a constant freshwater production rate of 2 kg/s, for desalination systems with 4, 8, and 12 effects, respectively.

Table 6, which corresponds to the four-effect desalination system, shows that increasing solar radiation leads to a clear improvement in the performance ratio across all feed water temperatures. The effect of solar radiation is more pronounced at intermediate feed water temperatures, particularly at $T_s = 100$ ˚C, where the system exhibits the highest sensitivity to changes in solar radiation. Under these conditions, the maximum variation in the performance ratio reaches approximately 21.06%.

Table 6. The variation of performance ratio (PR) versus solar radiation on the different feed water temperature at a fixed desalination effect of N=4

Q_{rad}(W/m²)	PR			
	T_s =80°C	T_s =90°C	T_s =100°C	T_s =110°C
0	4.00	3.97	3.94	3.91
800	4.62	4.60	4.58	4.55
1000	4.75	4.73	4.71	4.68
1100	4.75	4.79	4.77	4.75

In Table 7, representing the eight-effect configuration, the performance ratio continues to increase with intensifying solar radiation for all feed water temperatures. However, compared to the four-effect system, the relative variation of the performance ratio is reduced. This behavior can be attributed to enhanced internal heat recovery in systems with a higher number of effects, which diminishes the relative contribution of external solar energy.

Table 7. The variation of performance ratio (PR) versus solar radiation on the different feed water temperature at a fixed desalination effect of N=8

Q_{rad}(W/m²)	PR			
	T_s =80°C	T_s =90°C	T_s =100°C	T_s =110°C
0	8.02	7.97	7.93	7.88
800	9.29	9.26	9.22	9.19
1000	9.55	9.52	9.49	9.46
1100	9.68	9.65	9.62	9.59

Table 8 presents the results for the twelve-effect desalination system. Although the application of higher solar radiation still improves the performance ratio, the magnitude of variation is further reduced compared to the systems with fewer effects. This indicates that high-effect multi-stage desalination systems exhibit greater thermal stability and lower sensitivity to variations in solar radiation intensity. It should be noted that, as shown in Table 8, the performance ratio at a given solar radiation level decreases monotonically as the feed water temperature T_s increases from 80 ˚C to 110 ˚C, consistent with the sensitivity trend reported in Table 9; this is why the no-solar ($Q_{rad} = 0$) value at $T_s = 100$ ˚C and N=12 is lower than the corresponding value at $T_s = 80$ ˚C.

Table 8. The variation of performance ratio (PR) versus solar radiation on the different feed water temperature at a fixed desalination effect of N=12

Q_{rad}(W/m²)	PR			
	T_s =80°C	T_s =90°C	T_s =100°C	T_s =110°C
0	12.05	11.99	11.92	11.85
800	13.97	13.93	13.89	13.84
1000	14.37	14.33	14.29	14.25
1100	14.56	14.52	14.49	14.45

Overall, a comparative analysis of Tables (6)–(8) confirms that the maximum variation of the performance ratio due to solar radiation occurs in the four-effect system (N=4) at T_s=100 ˚C, while increasing the number of effects progressively reduces the influence of solar radiation owing to improved internal thermal efficiency. To evaluate the influence of input parameter variations on the system performance ratio, a sensitivity analysis was conducted based on the data presented in Tables 4 through 8. In this analysis, the effects of changes in solar radiation and feed water temperature on the performance ratio (PR) were examined, and the corresponding results are summarized in Table (9). The results in Table (9) indicate that the performance ratio is more sensitive to variations in solar radiation. Specifically, increasing solar radiation from 800 to 1000 W/m² leads to an approximate 2.7–3% increase in PR. In contrast, increasing the feed water temperature from 80 to 110 ˚C has a smaller impact, resulting in only a slight decrease in PR of about 1–2%. These findings demonstrate that solar radiation is a more influential parameter in enhancing the performance of the MED system.

Table 9. Sensitivity of the performance ratio (PR) to variations in solar radiation and feed water temperature

Parameter change	Configuration	% Change in PR
ΔQ_{rad} = 800 → 1000 W/m²	N = 4–12, T_s = 80–110 °C	2.7–3.0 % increase
ΔT_s = 80 → 110 °C	N = 8, Q_{rad} = 0–1100 W/m²	1–2 % decrease

5. Conclusion

In this study, the effects of direct solar radiation and the number of effects of multi-effect desalination are investigated. For this modeling, an accurate numerical-algebraic hybrid solution with parametric solution has been used. The most important results of this study can be abbreviated as:

- The results of the present algebraic model have an acceptable agreement with the published data [8] with maximum errors of 0.1% where this error is occurred in *N*=4.
- The trend of variation for temperature in the present model and numerical data [8] is unique.
- The performance ratio increases linearly as the number of desalination effects rises, regardless of feed water temperature or the level of direct solar radiation.
- The highest performance ratio in the no-solar condition was obtained for the 12-effect system at 80 ˚C, with a value of 12.05. Under solar radiation, the performance ratio can increase further to 14.56.
- With increasing solar radiation, the maximum increase in PR is 20.3% for a feed water temperature of 80 ˚C and *N*=12.
- Increasing solar radiation from 0 to 1100 W/m^2 enhances the performance ratio with maximum increases 22.1%, 20.1% and 19.5% for desalination effects of 4, 6 and 8.
- The maximum variation of PR for different solar radiation is 21.06% and occurred at T_s=100 ˚C and *N*=4.
- Sensitivity analysis shows that solar radiation is the dominant factor affecting PR, with a 2.7–3% increase for a radiation rise from 800 to 1000 W/m², while feed water temperature changes cause only minor (1–2%) variations.

Nomenclature

Symbols

A	Empirical coefficient in the boiling-point-elevation (BPE) correlation; also, effective solar-exposed surface area of an effect (m²)	T_f	Feed water temperature (°C)
B	Empirical coefficient in the BPE correlation	T_S	Motive (driving) steam temperature (°C)
B_i	Brine (reject) flow rate leaving effect I (kg/s)	$T_{effect(new)}$	Brine temperature after solar-energy absorption (°C)
BPE	Boiling point elevation (°C)	$T_{effect(old)}$	Brine temperature before solar-energy absorption (°C)
C	Empirical coefficient in the BPE correlation	X	Salinity (general term used in the BPE correlation) (ppm)
C_p	Specific heat capacity of water (kJ/kg.°C)	X_{b1}	Brine salinity leaving effect 1 (ppm)

D_i	Distillate (vapor) flow rate generated in effect *i* (kg/s)
d_i	Flash-evaporated vapor flow rate from the brine in effect *i* (kg/s)
d'_i	Condensed flash-vapor flow rate in effect *i* (kg/s)
F_i	Feed water flow rate entering effect *i* (kg/s)
i	Effect index ($i = 1, 2, \ldots, N$)
I	Incident direct solar irradiance (W/m²)
M_d	Total freshwater (distillate) production rate (kg/s)
M_{ev}	Mass flow rate of saturated vapor extracted from the last effect to the ejector (kg/s)
M_f	Total feed water mass flow rate (kg/s)
M_m	Mass flow rate of the driving (motive) steam (kg/s)
Ms	Equivalent motive steam flow rate used to evaluate PR (kg/s)
$\dot{m}$	Brine mass flow rate (solar-heating term) (kg/s)
N	Number of desalination effects
NEA_i	Non-equilibrium allowance in effect *i* (°C)
P_S	Motive steam pressure (kPa)
PR	Performance ratio
Q_Solar	Absorbed solar heat rate (W)
T_i	Temperature of effect *i* (°C)
T_{evi}	Vapor temperature entering the next effect after the demister pressure drop (°C)
T_{vi}	Vapor temperature produced in effect *i* (°C)
T'_i	Temperature of the liquid stream entering the flash-evaporation zone of effect *i* (°C)
T_0	Temperature of the vapor entering the first effect from the upstream stage (°C)
X_f	Feed water salinity (ppm)

Greek symbols

ΔT	Uniform temperature difference between two consecutive effects (°C)
ΔT_P	Temperature drop across the demister (°C)
ΔT_{loss}	Overall system temperature loss (°C)
A	Surface absorptivity
α_p	Effective absorptivity of the effect surface
T	Cover transmittance
Λ	Latent heat of vaporization (general, temperature-dependent) (kJ/kg)
λ_i	Latent heat of vaporization at the temperature of effect *i* (kJ/kg)
λ'_i	Latent heat of vaporization associated with flash evaporation in effect *i* (kJ/kg)
λ_S	Latent heat of vaporization of the motive (driving) steam kJ/kg
λ_{v1}	Latent heat of vaporization at the vapor temperature of effect 1 (kJ/kg)

Abbreviations

MED	Multi-Effect Distillation / Desalination
RO	Reverse Osmosis
TVC	Thermal Vapor Compression
GOR	Gained Output Ratio
BPE	Boiling Point Elevation
NEA	Non-Equilibrium Allowance
PR	Performance Ratio
CFD	Computational Fluid Dynamics

References

[1] Abdel-Rehim, Z.S., Lasheen, A., 2007. Experimental and theoretical study of a solar desalination system located in Cairo, Egypt, Desalination, 217 (1–3), 52–64. https://doi.org/10.1016/j.desal.2007.01.012

[2] Mistry, K.H., Antar, M.A., Lienhard, J.H., 2013. An improved model for multiple-effect distillation, Desalination and Water Treatment, 51 (4), 807–821. http://dx.doi.org/10.1080/19443994.2012.703383

[3] Jones, E., Qadir, M., van Vliet, M.T.H., Smakhtin, V., Kang, S., 2019. The state of desalination and brine production: A global outlook, Science of the Total Environment, 657, 1343–1356. https://doi.org/10.1016/j.scitotenv.2018.12.076

[4] Shenvi, S.S., Isloor, A.M., Ismail, A.F., 2015. A review on RO membrane technology: Developments and challenges, Desalination, 368, 1–16. https://doi.org/10.1016/j.desal.2014.12.042

[5] Huang, J., Zheng, H., Kong, H., 2024. Key pathways for efficient solar thermal desalination, Energy Conversion and Management, 299, 117806. https://doi.org/10.1016/j.enconman.2023.117806

[6] Hosseini, S., Karimi Shavaki, M.B., 2024. Analysis of energy and exergy and modeling of thermal water desalination coupled with combined cycle and solar power plant in hot and humid regions, AUT Journal of Mechanical Engineering. https://doi.org/10.22060/ajme.2024.23230.6117

[7] Sun, Q., Hu, X., Zhang, W., Wu, L., 2025. Optimization of membrane and thermal (MED-RO) hybrid desalination system, Journal of Water Process Engineering, 76, 108114. https://doi.org/10.1016/j.jwpe.2025.108114

[8] El-Dessouky, H.T., Ettouney, H.M., 2002. Fundamentals of Salt Water Desalination, 1st Edition, Elsevier Science, Amsterdam, The Netherlands (see Chapter 4, "Multiple Effect Evaporation," pp. 99–136, for the MEE thermal model).

[9] El-Dessouky, H.T., Ettouney, H.M., 1999. Multiple-effect evaporation desalination systems: Thermal analysis. Desalination, 125(1–3), 259–276. https://doi.org/10.1016/S0011-9164(99)00147

[10] El Sayed, Y.M., Silver, R.S., 2002. Fundamentals of distillation. In: Spiegler, K.S., Laird, A.D.K. (Eds.), Principles of Desalination, Academic Press, Part A, pp. 223–299 (or Chapter 5).

[11] Darwish, M.A., Abdulraheim, H.K., 2008. Feed water arrangements in a multi-effect desalting system, Desalination, 228, 30–54. https://doi.org/10.1016/j.desal.2007.05.039

[12] Druetta, P., Aguirre, P., Mussati, S., 2013. Optimization of multi-effect evaporation desalination plants, Desalination, 311, 1–15. http://dx.doi.org/10.1016/j.desal.2012.10.033

[13] Jyoti, G., Khanam, S., 2014. Simulation of heat-integrated multiple-effect evaporator system, International Journal of Thermal Sciences, 76, 110–117. https://doi.org/10.1016/j.ijthermalsci.2013.08.016

[14] Piacentino, A., Cardona, E., 2010. Advanced energetics of a multiple-effects evaporation (MEE) desalination plant. Part II: Potential prospects for cost formation and integration, Desalination, 259, 44–52. https://doi.org/10.1016/j.desal.2010.04.037

[15] Zhao, D., Xue, J., Li, S., Sun, H., Zhang, Q., 2011. Theoretical analyses of thermal and economical aspects of multi-effect distillation desalination dealing with high-salinity wastewater, Desalination, 273, 292–298. https://doi.org/10.1016/j.desal.2011.01.048
[16] El-Allawy, M., 2003. Predictive simulation of the performance of MED-TVC desalination distiller, Proceedings of the IDA World Congress, International Desalination Association, Bahamas.
[17] Aly, N.H., El-Figi, A.K., 2003. Thermal performance of seawater desalination systems, Desalination, 158, 127–142. https://doi.org/10.1016/S0011-9164(03)00443-0
[18] Ameri, M., Seif Mohammadi, S., Hosseini, M., Seifi, M., 2009. Effect of design parameters on multi-effect desalination system specifications, Desalination, 245, 266–283. https://doi.org/10.1016/j.desal.2008.07.012
[19] Casimiro, S., Cardoso, J., Alarcón-Padilla, D.C., Turchi, C., Ioakimidis, C., Mendes, J.F., 2014. Modeling multi-effect distillation powered by CSP in TRNSYS, Energy Procedia, 49, 2241–2250. https://doi.org/10.1016/j.egypro.2014.03.237
[20] Casimiro, S., Cardoso, J., Ioakimidis, C., Mendes, J., Mineo, C., Cipollina, A., 2014. MED parallel system powered by concentrating solar power (CSP): Model and case study (Trapani, Sicily), Desalination and Water Treatment, 55 (12), 3253–3266. https://doi.org/10.1080/19443994.2014.940222
[21] Azimibavil, S., Jafarian, A., 2016. Dynamic simulation of a multi-effect distillation (MED) process, Desalination, 392, 91–101. https://doi.org/10.1016/j.desal.2016.04.004
[22] Maha, B., Ali, S., Ammar, B.B., 2017. Modeling and simulation of multi-effect desalination plant (SIDEM unit), Proceedings of the International Conference on Green Energy Conversion Systems (GECS), Hammamet, Tunisia. https://doi.org/10.1109/GECS.2017.8066148
[23] Kamali, R.K., Abbassi, A., Sadough Vanini, S.A., Saffar Avval, M., 2008. Thermodynamic design and parametric study of MED-TVCM, Desalination, 222 (1–3), 596–604. https://doi.org/10.1016/j.desal.2007.01.120
[24] Kamali, R.K., Mohebinia, S., 2008. Experience of design and optimization of multi-effect desalination systems in Iran, Desalination, 222 (1–3), 639–645. https://doi.org/10.5004/dwt.2008.27157
[25] Abdi-Khanghah, M., Bazooyar, B., Gonbadi, M., Wu, K.C.W., 2023. Design and optimization of MED-TVC desalination plant using mathematical modeling coupled with response surface methodology, Journal of the Taiwan Institute of Chemical Engineers, 153, 105187. https://doi.org/10.1016/j.jtice.2023.105187
[26] Ahmadi, A., Noorpoor, A.R., Kani, A.R., Saraei, A., 2021. Modeling and economic analysis of MED-TVC desalination integrated with the Allam power plant cycle in Kish Island, Iran, Iranian Journal of Chemical and Chemical Engineering, 40 (6), 1882–1892. https://doi.org/10.30492/ijcce.2020.117914.3851
[27] Ghorbani, S., Deymi-Dashtebayaz, M., Taiyuan, E., 2023. Parametric investigation and performance optimization of a MED-TVC desalination system based on 1-D ejector modeling, Energy Conversion and Management, 288, 117131. https://doi.org/10.1016/j.enconman.2023.117131
[28] Sayyaadi, H., Saffari, A., 2010. Thermoeconomic optimization of multi-effect distillation desalination systems, Applied Energy, 87, 1122–1133. https://doi.org/10.1016/j.apenergy.2009.05.023
[29] Sayyaadi, H., Saffari, A., 2010. Various approaches in optimization of multi-effect distillation desalination systems using a hybrid meta-heuristic optimization tool, Desalination, 257, 138–148. https://doi.org/10.1016/j.desal.2009.11.045
[30] Al-Hotmani, O.M.A., Al-Obaidi, M.A., Filippini, G., Manenti, F., Patel, R., Mujtaba, I.M., 2020. Optimisation of multi-effect distillation based desalination system for minimum freshwater production cost via repetitive simulation, Computers & Chemical Engineering, 135, 106710. https://doi.org/10.1016/j.compchemeng.2019.106710
[31] Palenzuela, P., Hassan, A.S., Zaragoza, G., Alarcón-Padilla, D.-C., 2012. Steady state model for multi-effect distillation case study: Plataforma Solar de Almería MED pilot plant, Desalination and Water Treatment, 31 (1–3), 255–265. https://doi.org/10.1016/j.desal.2013.12.029
[32] Zamen, M., Kahani, M., Yazdanpanahi, J., Abedini, R., Ahmadi, M.H., 2023. Modeling of a direct-contact humidification–dehumidification desalination unit in a 256 MW steam power plant using effluent streams: Case study, Case Studies in Thermal Engineering, 45, 102966. https://doi.org/10.1016/j.csite.2023.102966
[33] Shahouni, R., Abbasi, M., Kord, M., Akrami, M., 2024. Modelling and optimising MED-TVC seawater desalination plants assisted with electric heaters, Water Resources and Industry, 32, 100262. https://doi.org/10.1016/j.wri.2024.100262
[34] Khonsha, I., 2026. Computational Fluid Dynamics Simulation for Predicting Pressure and Velocity Variations at Dry and Two-Phase States in Spinning Cone Column, Chemical Process Design, 5 (1), 42–53. http://doi.org/10.22111/cpd.2025.52360.1061
[35] Karishma, S., Jana, A.K., 2026. Multi-effect desalination: Dynamics, validation and optimization through diverse algorithmic frameworks, Separation and Purification Technology, 389, 136919. https://doi.org/10.1016/j.seppur.2026.136919